

# Implications of Higgs Sterility for the Higgs and Stop Sectors

Jun Guo,<sup>1,\*</sup> Zhaofeng Kang,<sup>2,†</sup> Jinmin Li,<sup>1,‡</sup> and Tianjun Li<sup>1,3,§</sup>

<sup>1</sup>*State Key Laboratory of Theoretical Physics and Kavli Institute for  
Theoretical Physics China (KITPC), Institute of Theoretical Physics,  
Chinese Academy of Sciences, Beijing 100190, P. R. China*

<sup>2</sup>*Center for High-Energy Physics, Peking University, Beijing, 100871, P. R. China*

<sup>3</sup>*School of Physical Electronics, University of Electronic Science  
and Technology of China, Chengdu 610054, P. R. China*

## Abstract

The LHC data implies that the newly discovered Higgs boson  $h$  may be sterile (highly SM-like). In supersymmetric SMs (SSMs), Higgs couplings are often modified by Higgs mixing and stop loop corrections, so we study the Higgs sterility in the Higgs and stop sectors in two SSMs: (I) The Minimal SSM (MSSM). In the nearly decoupling region, the doublet-doublet mixing effect can only enhance  $C_{h\bar{b}b}$  by  $2m_Z^2/M_A^2$ . Sterility places  $M_A \gtrsim 900$  GeV. But it hardly constrains the stop sector due to the heaviness of Higgs boson mass  $m_h$ ; (II) The next to MSSM (NMSSM). In the presence of doublet-singlet mixing, the mixing structure is complicated. We find a simple approximation to understand Higgs sterility and its implications, says the amount of pushing-up  $m_h \lesssim 5$  GeV while the pulling-down scenario is favored. Stops can be light here, so Higgs sterility significantly constrains them directly and indirectly except for blind spots. We also study the LHC features of the whole stop sector facing a sterile Higgs and find that, in virtue of decays between stops and sbottom, characteristic signatures like same-sign leptons and multi  $b$ -jets are promising probes.

PACS numbers:

---

\*Electronic address: hustgj@itp.ac.cn

†E-mail: zhaofengkang@gmail.com

‡Electronic address: jmli@itp.ac.cn

§Electronic address: tli@itp.ac.cn

## I. INTRODUCTION AND MOTIVATIONS

In the last two years, the ATLAS and CMS collaborations have established the discovery of a new resonance, putatively the long-sought standard model (SM)-like Higgs boson  $h$  [1]. It is a big milestone for the particle physics. The more precise measurements on its particle properties are still ongoing, but in light of the current data [1], we know that it has a mass  $m_h \simeq 126$  GeV (relatively heavy if interpreted in the minimal supersymmetric SM (MSSM)), and moreover its main signatures are consistent with the SM predictions very well.

Actually, the highly SM-like Higgs boson emerges as data accumulating. In the Higgs discovery, the channels with largest sensitivity are the four lepton channel  $h \rightarrow ZZ^* \rightarrow 4\ell$  and the di-photon channel  $h \rightarrow \gamma\gamma$ . The former does not show any significant deviation from the SM prediction. While the latter, despite of showing excess at the early stage, is steadily declining to the SM case. The fermionic channels such as  $h \rightarrow b\bar{b}$  and  $h \rightarrow \tau\bar{\tau}$  have smaller sensitivities, but the present hints of these channels indicate that their signal strengthes are also within the SM expectations [2]. Thereby, pessimistically speaking, we may have to face a highly SM-like Higgs boson (dubbed as sterile Higgs boson hereafter) in the near future. To quantify Higgs sterility, we refer the LHC best experimental resolution which is based on the 14 TeV LHC of  $300 \text{ fb}^{-1}$ , for instance [3]

$$\frac{\Delta(\sigma_{\text{GF}}\text{Br}(2\gamma))}{\sigma_{\text{GF}}\text{Br}(2\gamma)} : 0.06, \quad \frac{\Delta(\sigma_{\text{GF}}\text{Br}(ZZ))}{\sigma_{\text{GF}}\text{Br}(ZZ)} : 0.09. \quad (1)$$

Resolution of ILC can be as good as 1%, but the current numerical tools can not match that. Thus, for main channels a deviation  $\lesssim 10\%$  is a reasonable range of sterility.

As been well known, the Higgs signatures can be utilized to probe new physics beyond the SM, e.g., the Higgs mixing with other states, couplings to extra charged particles, and decaying into extra light particles. As a matter of fact, all of them, especially the first and second cases, occur in the supersymmetric SMs (SSMs). In the SSMs, the SM Higgs sector is extended by another Higgs doublet like in the minimal SSM (MSSM), and maybe one more singlet in the next to MSSM (NMSSM) [4] (or triplet [5, 6]). Hence Higgs doublet-doublet and doublet-singlet mixing (DSM) are expected. Moreover, the stop sector, which significantly couples to  $h$ , has effects on the Higgs mass and couplings as well. Therefore, it is of importance to investigate implications of Higgs sterility on the Higgs and stop sector. In this paper we analytically analyze the feature of doublet-doublet mixing in the MSSM, and how it is affected by DSM in the NMSSM. It is found that the doublet-doublet mixing effect decouples as  $1/M_A^2$  and  $\tan\beta/M_A^2$ , respectively. Owing to  $m_h$ , in the MSSM the stop sector should be heavy and is thus hardly constrained by Higgs sterility, except in some limiting case. By contrast, in the NMSSM the whole stop sector can be fairly light, so sterility acts. Besides, DSM can push-up or pull-down  $m_h$ , with a degree bounded by Higgs sterility, as

means that the stop sector is also indirectly influenced by sterility.

With the resulted light stop ensemble which contains two stops and light sbottom, we are interested in their LHC profiles. They potentially provide a new angle on stop searches at the LHC. For instance, generically speaking decays between stops and sbottom are kinematically allowed and with large branching ratios, so a hard  $W$  or  $Z$  boson is produced. Taking into account the possible top quark from the lightest stop decay, we thus expect signatures with same sign leptons plus missing energy at the LHC. From our preliminary analysis, this is a promising probe for the stop ensemble.

This paper is organized as follows. In Section II we investigate implications of a sterile Higgs boson around 126 GeV on the Higgs and stop sector, of the MSSM and NMSSM respectively. In the next section an anatomy of the stop sector facing such a Higgs boson is made. We analyze the decays of the stop ensemble and preliminarily explore their characteristic signatures at the LHC. Discussion and conclusion are casted in Section IV and some necessary and complementary details are given in the Appendices.

## II. IMPLICATIONS OF A STERILE HIGGS BOSON IN THE MSSM AND NMSSM

The current data may point to a Higgs boson with highly SM-like couplings, so seemingly it does not convey much information of new physics to us. Such a sterile Higgs boson places stringent bounds on Higgs couplings which, in the SSMs, tend to show deviations from the SM predication. In this section, taking the MSSM and NMSSM as examples, we investigate implications of Higgs sterility on the Higgs sector, which exhibits Higgs mixings, and on the stop sector, which has a notable effect on both mass and couplings of the Higgs boson. Numerical study is employed as well.

### A. A sterile Higgs boson in the MSSM

In the MSSM we have two Higgs doublets  $H_u$  and  $H_d$ . The mixing effects between them are not difficult to be analyzed. They lead to the tree-level reduced couplings of the SM-like Higgs boson (All notations are casted in Appendix A.):

$$C_V = \sin(\beta - \alpha), \quad C_t = \frac{\cos \alpha}{\sin \beta}, \quad C_{hb\bar{b}} = -\frac{\sin \alpha}{\cos \beta}, \quad (2)$$

with  $\tan \beta = v_u/v_d$ . The mixing angle between the heavy and light (SM-like) CP-even Higgs boson  $\alpha$  is given by [7]

$$-\pi/2 \leq \alpha = \frac{1}{2} \arctan \left[ \tan 2\beta (M_A^2 + m_Z^2)/(M_A^2 - m_Z^2) \right] \leq 0. \quad (3)$$

In the nearly decoupling region  $M_A^2 \gg m_Z^2$  and  $\tan \beta \gg 1$ , the expressions in Eq. (4) are approximated to be [7]

$$C_V \rightarrow 1 - \frac{2m_Z^4}{M_A^4 \tan^2 \beta}, \quad C_t = 1 - \frac{2m_Z^2}{M_A^2 \tan^2 \beta}, \quad C_{hb\bar{b}} = 1 + \frac{2m_Z^2}{M_A^2}. \quad (4)$$

As one can see, only  $C_{hb\bar{b}}$  can be appreciably affected, concretely speaking, enhanced. In that case, the MSSM predicts a universal suppression of the signature strengths except for these involving  $b\bar{b}$  which should be close to unit [51]. From the first panel of Fig. 1 it is seen that, to meet Higgs sterility we need to set  $M_A \gtrsim 900$  GeV. This is obviously heavier than the tree-level estimation  $\gtrsim 600$  GeV, owing to the radiative correction which is enhanced by a large  $\tan \beta$  [7].

We now turn to the implication of Higgs sterility on the stop sector. It is well known, due to the significant coupling to  $H_u$ , the stop sector plays a crucial role in moulding properties of the SM-like Higgs boson. Firstly, it is related to origins of the Higgs boson mass. In SSMS the Higgs boson mass can be expressed as

$$m_h^2 = (m_Z^2 \cos^2 2\beta + \Delta m_h^2) + m_Z^2 f(\lambda, \beta). \quad (5)$$

The first term is predicted by the MSSM. It consists of the tree-level contribution from Higgs quartic term, determined by D-terms, as well as the stop radiative correction

$$\Delta m_h^2 = \frac{3m_t^4}{4\pi^2 v^2} \left[ \log \frac{m_t^2}{m_{\tilde{t}}^2} + \frac{X_t^2}{m_{\tilde{t}}^2} \left( 1 - \frac{X_t^2}{12m_{\tilde{t}}^2} \right) \right], \quad (6)$$

with the average stop mass  $m_{\tilde{t}} = \sqrt{m_{\tilde{t}_1} m_{\tilde{t}_2}}$  (Stop parameters are defined in Appendix B). The second term denotes contributions from extra tree-level Higgs quartic terms such as in the NMSSM discussed below. Secondly, stops, which carry both QCD and QED charges, modify the Higgs effective couplings to gluons and photons, e.g., by a shift in the Higgs-gluon reduced coupling [9, 10]

$$\delta C_{hGG} = \frac{\delta r_g}{r_{\text{SM},g}} \approx 1 + \frac{1}{4} \left( \frac{m_t^2}{m_{\tilde{t}_1}^2} + \frac{m_t^2}{m_{\tilde{t}_2}^2} - \frac{X_t^2 m_t^2}{m_{\tilde{t}}^2 m_{\tilde{t}}^2} \right). \quad (7)$$

The convention can be found in Appendix. A. Therefore, with light stops or/and large stop mixing, Higgs sterility may be violated.

In the MSSM almost half of  $m_h$  origins from the stop radiative correction. To achieve a large  $\Delta m_h^2$  and keep stops as light as possible at the same time, we have to rely on a large stop mixing, says in the stop maximal mixing scenario with  $X_t^2 \simeq 6m_{\tilde{t}}^2$ . Light stops are chased after for the sake of both naturalness and their detection at the LHC. Then Higgs sterility excludes a part of the parameter space of light stops. We would like to stress that,



light stops and large stop mixing may result in a substantial cancelation between terms in the bracket of Eq. (7), so a blind spot exists in Higgs sterility. In other words, light stops may hide behind the sterile Higgs boson. It is straightforward to derive the condition for that:

$$m_{\tilde{t}_1}^2 + m_{\tilde{t}_2}^2 = m_{LL}^2 + m_{RR}^2 = X_t^2. \quad (8)$$

The top left panel of Fig. 2 shows that Higgs sterility is absolutely null and void. However, it is not always the case. It is blamed to our parameter setting for the stop sector shown in Eq. (17), which just drives the light stop around 350 GeV into the blind spots. In principle, one light stop is allowed to be rather light if we set another stop very heavy.

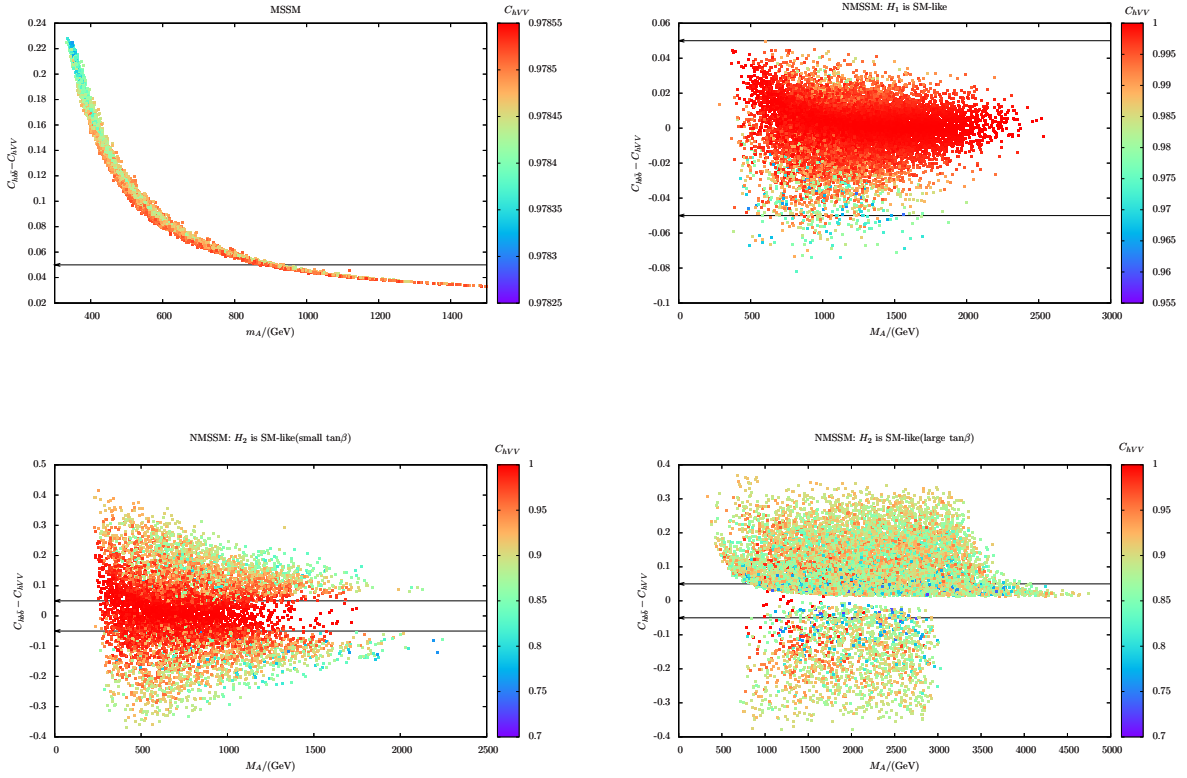


FIG. 1: Inspecting Higgs sterility on the  $\tilde{C}_{hbb} - M_A$  plane, with color code denoting  $C_{hVV}$ . The reduced couplings with a tilde are subtracted by  $C_{hVV}$  so as to isolate the universal mixing effect. Top left: MSSM; Top Right: NMSSM in the pulling-down scenario; Bottom left/right: NMSSM in the pushing-up scenario with a small/large  $\tan\beta$ .

## B. A sterile Higgs boson in the NMSSM

The Higgs sector of the NMSSM is further extended by a singlet  $S$ , which dramatically changes the Higgs phenomenologies. Above all, it is able to enhance  $m_h \simeq 126$  GeV without turning to heavy stops and thus is regarded as a benchmark model for natural SUSY [11]. The Higgs sector of the model, in the scale invariant form, is given by

$$\begin{aligned} W \supset & \lambda S H_u \cdot H_d + \frac{\kappa}{3} S^3, \\ -\mathcal{L}_{soft} \supset & \lambda A_\lambda S H_u \cdot H_d + \frac{\kappa}{3} A_\kappa S^3 + h.c. \end{aligned} \quad (9)$$

There are three CP-even Higgs bosons out of this Higgs sector. To understand Higgs mixing and mass, it is convenient to work in a basis defined as [13, 14]

$$H_u^0 = v_u + \frac{1}{\sqrt{2}} (S_1 \cos \beta + S_2 \sin \beta), \quad H_d^0 = v_d + \frac{1}{\sqrt{2}} (S_1 \sin \beta - S_2 \cos \beta), \quad H_S = v_s + \frac{S_3}{\sqrt{2}}, \quad (10)$$

The mass eigenstates  $H_{i=1,2,3}$  (masses in ascending order) are related with  $S_i$  via  $O$ , which is defined through  $OM_S^2O^T = \text{Diag}(m_{H_3}^2, m_{H_2}^2, m_{H_1}^2)$  with  $M_S^2$  the Higgs mass square matrix in the basis defined above (entries of  $M_S^2$  see Appendix. B). Neglecting mixing effects, the tree-level  $m_h$  is nothing but  $(M_S^2)_{22}$  which is a function of  $\lambda$  and  $\tan \beta$ , namely in Eq. (5)

$$f = \lambda^2 \sin^2 2\beta / g^2. \quad (11)$$

Plotting the contour of  $m_h$  on the  $\tan \beta - \lambda$  plane,  $\lambda = (g_1^2 + g_2^2)^{1/2} \approx 0.53$  is a critical line (Along it  $m_h$  independes on  $\tan \beta$ ): For  $\lambda > 0.53$ , the large  $\lambda$ -effect is working, and lowering  $\tan \beta$  helps to enhance  $m_h (> m_Z)$ ; While for  $\lambda < 0.53$  the situation is opposite. But the doublet-singlet mixing (DSM) effect modifies  $m_h$ , which will be discussed soon later.

With DSM, studying features of Higgs signature in the NMSSM is much more complicated than that of the MSSM (See some related works [16, 29]). But we find that for our purpose, the main features can be manifested by means of a simple approximate method. For definiteness, we focus on  $h = H_2$  and the case with  $h = H_1$  can be discussed similarly. Then the reduced couplings of  $H_2$  at tree-level are calculated to be

$$C_{2,V} = O_{22}, \quad C_{2,t} \simeq O_{22} + O_{21} \cot \beta, \quad C_{2,b} = O_{22} - O_{21} \tan \beta. \quad (12)$$

In most cases,  $O_{21} \cot \beta \ll 1$  can be safely neglected, and thus we get the universal reduction factor  $C_{2,V} \approx C_{2,t} = O_{22} < 1$ , which is mostly ascribed to DSM. The doublet-doublet mixing along with the DSM violate that universality by allowing a widely varied  $C_{2,b}$ . Moreover, it is noticed that as opposed to that of the MSSM, here  $C_{2,b}$  can be either larger or smaller than unit. To see this, we make use of the equation  $O_{1i}(M_S^2)_{ij}O_{2j} = 0$  to find out  $O_{21} \tan \beta$  at the leading order:

$$-O_{21} \tan \beta \simeq -\sin^2 \beta \cos 2\beta \frac{2(m_Z^2 - \lambda^2 v^2)}{M_A^2} - \tan \beta \frac{O_{13}(M_S^2)_{23} + O_{23}(M_S^2)_{13}}{M_A^2}. \quad (13)$$

This simple formula reveals the impact of DSM. When  $\tan\beta \gg 1$ , the first term reproduces its corresponding expression given in Eq. (4), up to the replacement  $m_Z^2 \rightarrow m_Z^2 - \lambda^2 v^2$ . Thus, given  $\lambda \gtrsim 0.6$  this term becomes negative. It is one of the difference between the MSSM and NMSSM, but is attributed to the new quartic term rather than DSM. The DSM effect is encoded in the second term of Eq. (13). One can find that, when we have a small  $\tan\beta \sim 1$  and moreover a properly light  $M_A$  (not as light as the one considered in the Ref. [15]), the second term tends to be dominant. But it has an indefinite sign, and consequently  $\Gamma(h \rightarrow b\bar{b})$  may be either increased or decreased. To show how does the DSM effect change Higgs signatures, we give the signature strength of Higgs to di-photon in the gluon fusion channel:

$$R_{gg}^{H_2}(\gamma\gamma) \approx O_{22}^2 \frac{1 + 2(\delta r_{2,g} + \delta r_{2,\gamma}/r_{SM,\gamma})/O_{22}}{1 - 1.17 \tan\beta O_{21}/O_{22} + 0.18 \delta r_{2,g}/O_{22}}, \quad (14)$$

where the stop contributions have been formally took into account. In summary, mixings in the NMSSM and MSSM are similar in the sense of the importance of  $C_{hb\bar{b}}$ , however, their quantitative consequences are noticeably different. In particular, the DSM effect in  $O_{21} \tan\beta$  is enhanced by a large  $\tan\beta$ , which makes it decouple not as  $1/M_A^2$  but as  $\tan\beta/M_A^2$ . As a result, it may be still significant even for  $M_A \gtrsim 3$  TeV, see the bottom-right panel of Fig. 1.

DSM influences not only the Higgs couplings but also Higgs mass. Concretely, the DSM effect pushes-up or pulls-down  $m_h$  [11, 17, 18], depending on  $H_2 = h$  or  $H_1 = h$ . In what follows we will investigate implications of Higgs sterility on each scenario, respectively.

**Revisit to the pushing-up scenario facing a sterile Higgs** We first consider  $H_2 = h$ , namely the pushing-up scenario which is characterized by an even lighter (than  $H_2$ ) CP-even Higgs boson  $H_1$  [52]. Realization of this scenario is important. First of all, it requires  $(M_S^2)_{22} > (M_S^2)_{33}$ . From Eq. (B2) it is seen that a moderately small  $\mu$  and not too large  $\kappa/\lambda$  are favored to make  $(M_S^2)_{33}$  sufficiently small. Furthermore, a properly large doublet-singlet mixing term  $(M_S^2)_{23}$  [11] is needed: On the one hand, it should be large enough to guarantee a sizable  $\Delta m_h$ ; On the other hand, it should be small enough to prevent a tachyon. Then typically we need

$$(M_S^2)_{23} = 2\lambda\mu v \left[ 1 - \left( \frac{A_\lambda}{2\mu} + \frac{\kappa}{\lambda} \right) \sin 2\beta \right] \sim \mathcal{O}(1000) \text{ GeV}^2, \quad (15)$$

except very degenerate  $(M_S^2)_{22}$  and  $(M_S^2)_{33}$ . Thereby, the region with  $\lambda \sim 1$ ,  $\tan\beta \sim 1$  and  $\mu \sim 200$  GeV accords well with the pushing-up scenario. Actually, this region takes full advantage of NMSSM effects to enhance  $m_h$  and is extensively studied [11, 18, 20]. But even for a larger  $\tan\beta$  and/or smaller  $\lambda$ , one can still turn to a large (but not

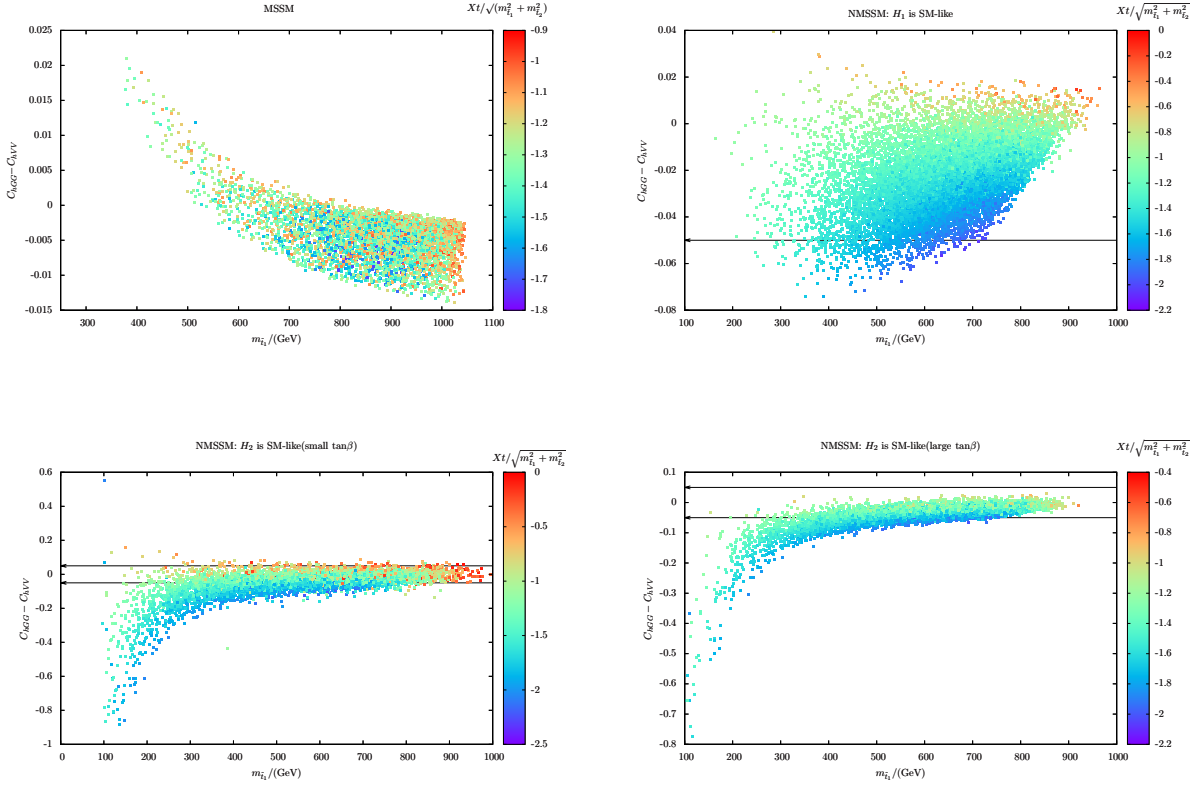


FIG. 2: Inspecting Higgs sterility on the  $\tilde{C}_{hGG} - m_{\tilde{t}_1}$  plane, with color code denoting the quantity  $X_t / \sqrt{m_{t_1}^2 + m_{t_2}^2}$  which reflects blindness of sterility. Figures are ordered the same with Fig. 1.

exceedingly large)  $A_\lambda$  to compensate their suppression on  $(M_S^2)_{23}$  and thus give a sizable pushing-up effect [53]. The right panel of Fig. 3 confirms the analysis.

We are at the position to quantify the pushing-up effect. Ref. [11] took an approximate method. It starts from the previously defined basis, in which the doublet sector has been approximately diagonalized, with two eigenvalues  $(M_S^2)_{22}$  and  $(M_S^2)_{11} (> (M_S^2)_{22})$  and the lighter state being the dominant component of  $h$ . It decouples the heavier state and discusses the DSM effect in the latter  $2 \times 2$  submatrix of  $M_S^2$ . This treatment neglects other DSM effects, which may be important especially in the region with a relatively small  $M_A$  and  $\tan\beta$ . In this work we instead use a numerical method. We diagonalise first the doublet sector then the full mass matrix, and each time get the SM-like Higgs boson mass  $m_{h'}$  and  $m_h$ , respectively. Then the DSM pushing-up effect can be measured by

$$\Delta m_h \equiv m_h - m_{h'}, \quad (16)$$

which is the exact result, including all DSM effects. Since the amount of pushing-up,

$\Delta m_h$ , is related to DSM, a sterile Higgs boson raises doubts about it. With numerical results we will find that, after imposing Higgs sterility (and the LEP upper bound [21] on  $H_1$  as well), the resulted pushing-up effect is indeed mild, typically  $\Delta m_h \lesssim 5$  GeV. This can be clearly seen in Fig. 3.

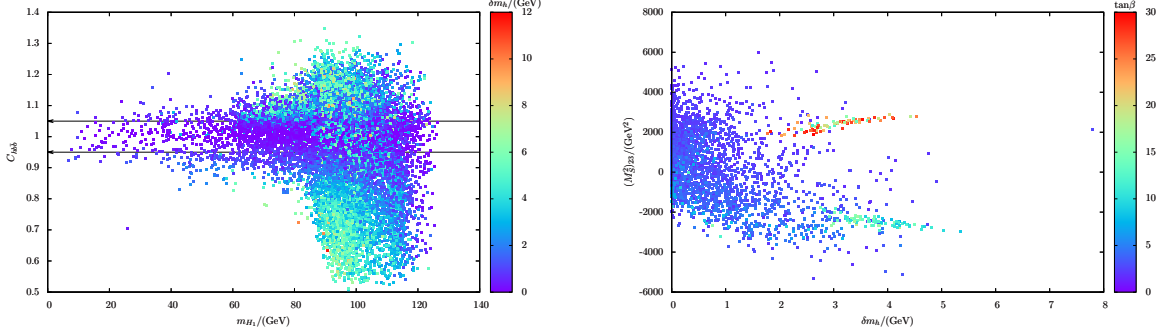


FIG. 3: Left panel: Distribution of  $\delta m_h$  on the  $\tilde{C}_{hb\bar{b}} - m_{H_1}$  plane; Right panel:  $\delta m_h$  versus doublet-singlet mixing element  $(M_S^2)_{23}$ , with color code denoting  $\tan \beta$ .

**Is the pulling-down region favored?** We now turn our attention to the case  $(M_S^2)_{22} < (M_S^2)_{33}$ . Then  $h = H_1$  and we confront with the pulling-down effect. The reduced couplings  $C_{1,X}$  can be derived analogue to  $C_{2,X}$ . To weaken the pulling-down effect to the most extent, one generically expects a smaller DSM, which implies a suppressed DSM effect on  $C_{1,b}$  (more precisely,  $O_{31} \tan \beta$ ). Moreover, compared to the MSSM, in this scenario the doublet-doublet mixing effect  $\simeq 2m_Z^2/M_A^2$  is also considerably attenuated, by the new large quartic term  $\lambda^2 v^2$  and a small  $\tan \beta$  as well (See the first term of Eq. (13)). Therefore,  $O_{31} \tan \beta$  is slight and becomes slighter as  $m_h$  becomes heavier. This explains why in the pulling-down scenario the Higgs di-photon excess for a 126 GeV Higgs boson is not significant [11]. However, viewing from Higgs sterility, this scenario is favored. It is manifest in the top right of Fig. 2, where Higgs sterility is almost automatically implemented. In addition, in this scenario the LEP bound does not concern us.

If  $\lambda \ll 1$ , we essentially go to the MSSM limit, which has been discussed above. So we only consider the large  $\lambda$  and small  $\tan \beta$  case, which retains the  $\lambda$ -effect to enhance  $m_h$  and hence we do not badly need heavy stops.

Since the NMSSM readily accommodates a light stop sector, direct constraints from Higgs sterility is powerful here. Recalling that DSM has effects on  $m_h$ , thus Higgs sterility is able to indirectly constrain the stop sector. This kind of constraint is most remarkable in the

region where the  $\lambda$ -effect is moderate or even negligible and then we rely on the pushing-up effect and stop radiative correction. To check that we compare the pushing-up scenario with a large  $\tan\beta$  and small  $\tan\beta$  (see Fig. 2): Before imposing the Higgs sterility bound, both cases allow a light stop  $\sim 100$  GeV, but imposing the bound (largely) excludes  $m_{\tilde{t}_1} < 250$  GeV and 150 GeV, respectively. Note that as explained before, a light stop may lie in the blind spot of Higgs sterility and thus is not excluded.

To end up this subsection, we would like to make a comment on the relationships among the DSM effect, its modification on the signatures and mass of Higgs boson. A significant DSM effect is reflected in  $O_{22}$  which shows a deviation from 1, as well as in  $O_{23,32}$  which should be relatively large. Generically, it would lead to an universal suppression of Higgs signature strengths, by  $O_{22}^2$ . However, in some cases the DSM effect, as shown previously, can distort  $C_{2b}$  such that the total decay width of Higgs boson decreases substantially, and then some of strengths such as di-photon rate are enhanced [18, 20]. But such kind of effect decouples for a sufficiently heavy  $M_A$ . The DSM impacts on  $m_h$ , with the degree determined by several factors, including  $O_{23,32}$ . But a large degree never necessarily means that  $O_{21} \tan\beta$  is large (See the left panel of Fig. 3). After clarifying these, we employ numerical study in the rest of this section.

### C. Numerical studies

In the MSSM we use HDECAY [22] and CALHEP [23] to calculate Higgs signatures and stop decays, respectively. And NMSSMtools 2.3 [24] is used for the relevant calculations in the NMSSM. In terms of the previous analysis, we set scanning parameters as the following:

$$\begin{aligned}
\text{MSSM : } \quad & \tan\beta : [5, 30], \quad \mu : [100, 1000] \text{ GeV}, \quad M_A : [300, 1500] \text{ GeV}, \\
& m_{\tilde{q}_3} : [300, 1000] \text{ GeV}, \quad m_{\tilde{u}_3} : [800, 2000] \text{ GeV}, \quad A_t : [-3000, -1500] \text{ GeV}. \\
\text{NMSSM : } \quad & \tan\beta : [1, 30], \quad \lambda : [0.1, 0.72], \quad \kappa : [0.01, 0.7], \\
& \mu : [100, 500] \text{ GeV}, \quad A_\lambda : [0, 3000] \text{ GeV}, \quad A_\kappa : [-600, 100] \text{ GeV}, \\
& m_{\tilde{q}_3}, m_{\tilde{u}_3} : [100, 1000] \text{ GeV}, \quad A_t : [-3000, 0] \text{ GeV}.
\end{aligned} \tag{17}$$

The SM-like Higgs boson mass is restricted to the region  $123 \text{ GeV} \lesssim m_h \lesssim 128 \text{ GeV}$ .  $\lambda \lesssim 0.72$  is required by perturbativity at the GUT scale. In the MSSM the stop soft masses squared are asymmetric, with  $m_{\tilde{q}_3}$  comparatively light so as to keep one stop and sbottom in the lower mass region. The soft mass squares of the third generation are relatively small so that the stops and the sbottom can be copiously produced at the 14 TeV LHC. As for

the other sparticles, we fix their soft masses to be

$$\begin{aligned} m_{\tilde{b}_R} &= 3000 \text{ GeV}, & m_{\tilde{q}_{1,2}} &= 2000 \text{ GeV}, & m_{\tilde{l}} &= 1000 \text{ GeV} \\ M_1 &= 250 \text{ GeV}, & M_1 : M_2 : M_3 &= 1 : 2 : 6. \end{aligned} \quad (18)$$

Thus the light sparticles which are relevant to our study include stops, the lighter sbottom, Higgsinos and gauginos. Such a setup keeps the number of parameters as small as possible, and moreover accords with natural SUSY. Results are displayed in the individual subsections, including figures from Fig. 1 to Fig. 6.

### III. THE STOP ENSEMBLE AT THE LHC

As one of the main object for this article, we will make an anatomy of the stop system under the condition of a sterile Higgs boson around 126 GeV. To implement Higgs sterility, we only keep the points (obtained in the previous section) which satisfy

$$0.9 \leq R_{\text{VBF}}(b\bar{b}, VV), \quad R_{\text{gg}}(\gamma\gamma, VV) \leq 1.1. \quad (19)$$

The heavier stop and lighter sbottom, which have not been extensively studied yet, will gain special attentions here. It is found that novel signatures from the heavier stop/sbottom cascade decays may be seen at the LHC. We will focus on the benchmark model for natural SUSY, the NMSSM, which provides a good laboratory to study the light stop ensemble facing a sterile Higgs boson. In terms of the setup for the stop sector, we have the following mass orders:

$$m_{\tilde{t}_1} < m_{\tilde{b}_1} \approx m_{\tilde{Q}_3} < m_{\tilde{t}_2}. \quad (20)$$

Their mass splittings are expected to be large, because a large  $X_t$  is favored by a relatively heavy  $m_h$ . Of course, altering the configuration of stop parameters leads to different distributions of mass spectra and decay widths, but that will not cause much difference to our discussions on the general features of the stop ensemble at the LHC.

In the rest of this section, we will first present the distributions of masses and decays of stops and sbottom, and then explore new signatures at the LHC. All of the discussions are based on the NMSSM unless otherwise specified. In fact, even disregarding their intimate connections with the Higgs boson properties and just for inspecting naturalness alone, our attempt is meaningful.

#### A. Decays of two stops and light sbottom

We now report the distributions of the main decay modes of  $\tilde{t}_{1,2}$  and  $\tilde{b}_1$ , respectively. In the discussion of Higgs mixing in the NMSSM, we divide it into several distinctive cases.



But decays of stop/sbottom do not show qualitative differences in different cases, so we only display results of the pulling-down scenario in this model, which is favored by Higgs sterility.

**On  $\tilde{t}_1$**  Distributions of the main decay branching ratios of  $\tilde{t}_1$  in Fig. 4. From it we make a few observations. In the lighter stop mass region,  $m_{\tilde{t}_1} \lesssim 500$  GeV, the mode  $\tilde{t}_1 \rightarrow b\tilde{\chi}_1^\pm$  (via the  $\tilde{t}_R$  component) usually has a larger branching ratio than others, such as that of  $\tilde{t}_1 \rightarrow t\tilde{\chi}_1^0$ . And its LHC bound is not strong if the masses of  $\tilde{\chi}_1^\pm$  and  $\tilde{\chi}_1^0$  are neither degenerate [26] nor hierarchical [27]. As a matter of fact, the current LHC exclusion on light stops is not our concern here [28], since that depends on the detailed models, e.g., whether  $R$ -parity is violated or not. In the heavier stop mass region,  $\tilde{t}_1 \rightarrow t\tilde{\chi}_{i>1}^0$  has a similar branching ratio with  $\text{Br}(\tilde{t}_1 \rightarrow b\tilde{\chi}_{i>1}^\pm)$ , while other modes are suppressed.

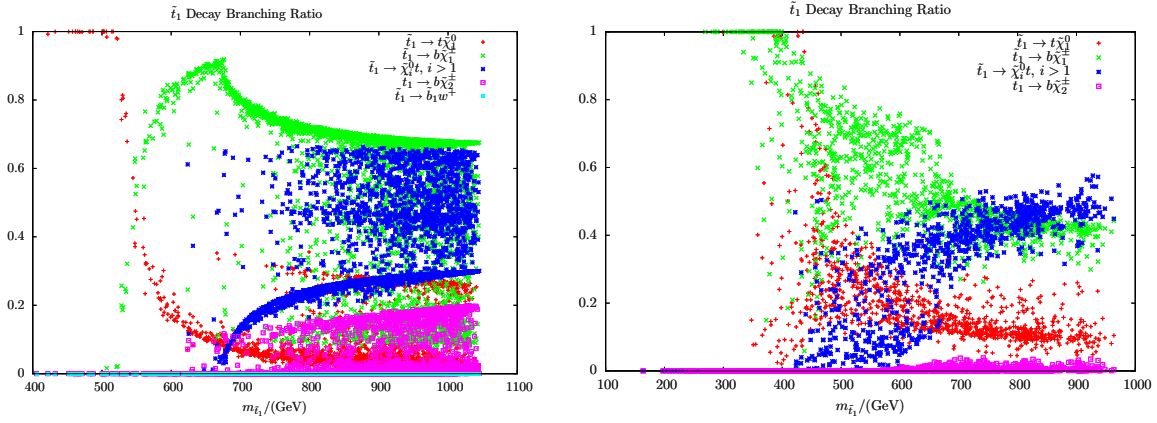


FIG. 4: Plots of decay branching ratios of  $\tilde{t}_1$ . Left panel: MSSM; Right panel: NMSSM in the pulling-down region. Other scenarios of the NMSSM give similar results, and differ mainly in the stop mass. So they are not shown explicitly.

**On  $\tilde{b}_1$**  In our setup, the sbottom mass can be as low as 200 GeV. As  $\tilde{t}_1$ , we keep an open attitude on the LHC bounds on that light sbottom. On  $\tilde{b}_1$  decays, the modes  $\tilde{b}_1 \rightarrow \chi_1^0 b$  and  $\tilde{b}_1 \rightarrow \sum_{i \geq 2} \chi_i^0 b$  almost take over the lower mass region of  $\tilde{b}_1$  (below about  $\sim 400$  GeV). While  $\tilde{b}_1 \rightarrow \chi_1^\pm t$  and  $\tilde{b}_1 \rightarrow \tilde{t}_1 W^\pm$  are dominant over the heavier sbottom region. The latter mode is in our interest in the ensuing discussions, so we give the analytical expression of its decay width at tree level (The complete one-loop correction on it can be found in Ref. [30]):

$$\Gamma(\tilde{b}_1 \rightarrow \tilde{t}_1 W) = \frac{g_2^2 \cos^2 \theta_t}{32\pi} \frac{m_{\tilde{b}_1}^3}{m_W^2} \lambda(m_{\tilde{b}_1}, m_{\tilde{t}_1}, m_W)^{3/2}. \quad (21)$$

with

$$\lambda(x, y, z) \equiv \left[ 1 - \left( \frac{y+z}{x} \right)^2 \right] \left[ 1 - \left( \frac{y-z}{x} \right)^2 \right]. \quad (22)$$

So the relative weights of these two modes are sensitive to the constituent of  $\tilde{t}_1$  and the mass splitting between  $\tilde{t}_1$  and  $\tilde{b}_1$ . As  $\tilde{b}_1$  becomes sufficiently heavy (typically heavier than 700 GeV for our choice of wino mass, 500 GeV), its decays to  $\chi_2^\pm t$  has a branching ratio a few tens of percents.

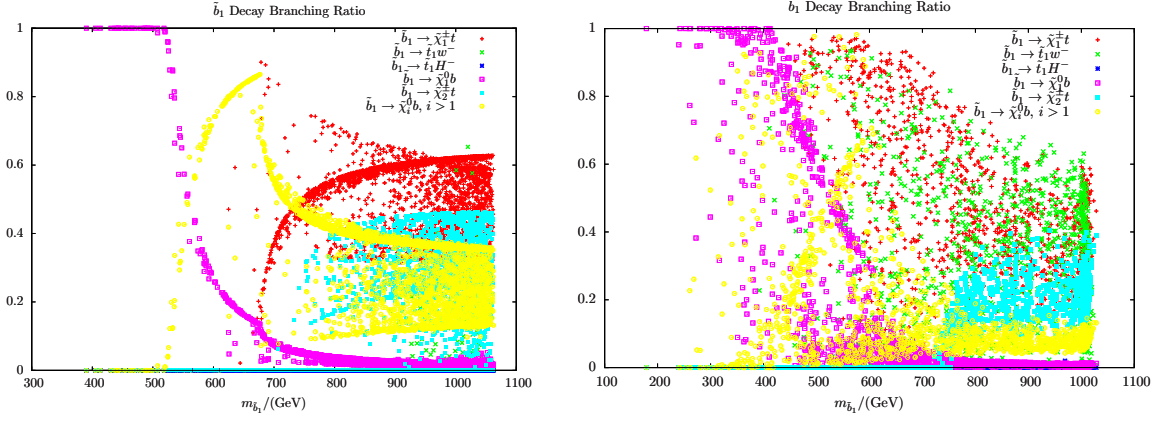


FIG. 5: Plots of decay branching ratios of  $\tilde{b}_1$ . Left: MSSM; Right: NMSSM.

**On  $\tilde{t}_2$**  It is the heaviest particle (with mass roughly above 600 GeV) of the stop ensemble, and consequently it possesses a rich decay table. That may impede the discovery of this particle due to the suppressed decay branching ratios of the individual channels. From Fig. 6 we see that, the conventional decay modes, i.e., to neutralinos and charginos, usually are subdominant (typically with branching ratios less than 20%), except that  $\tilde{t}_2 \rightarrow \sum_{i \geq 2} \chi_i^0 t$  takes up a larger branching ratio. Remarkably, the interesting modes  $\tilde{t}_1 Z/h$  and  $\tilde{b}_1 W^\pm$  have substantial branching ratios. For illustration, the partial decay widths of  $\tilde{t}_2$  to  $\tilde{t}_1$  plus  $Z$  and  $h$  are respectively given by

$$\Gamma(\tilde{t}_2 \rightarrow \tilde{t}_1 Z/h) \approx \frac{g_2^2}{\cos^2 \theta_W} \frac{\sin^2 2\theta_{\tilde{t}}}{256\pi} \frac{m_{\tilde{t}_2}^3}{m_Z^2} \lambda^{3/2}(m_{\tilde{t}_2}, m_{\tilde{t}_1}, m_Z), \quad (23)$$

$$\approx \frac{\cos^2 2\theta_{\tilde{t}}}{16\pi} \left( \frac{y_t^2 A_t^2}{m_{\tilde{t}}^2} \frac{m_{\tilde{t}_1}}{m_{\tilde{t}_2}} \right) m_{\tilde{t}_2}. \quad (24)$$

where we have taken  $H_u^0 \sim h$ . The  $Z$ -mode favors a large left-right (LR) stop mixing while the  $h$ -mode, which mainly is induced by the trilinear soft term ( $y_t A_t \tilde{Q}_3 H_u \tilde{U}_3^c + c.c.$ ), favors LR stops decoupling, says due to hierarchal stop soft masses squared. From Fig. 6 we find that,  $\text{Br}(\tilde{t}_2 \rightarrow \tilde{t}_1 Z) \sim 30\%$  in the total mass region of  $\tilde{t}_2$ , and  $\text{Br}(\tilde{t}_2 \rightarrow \tilde{t}_1 h)$  almost evenly scatters below the 30% line. As for  $\Gamma(\tilde{t}_2 \rightarrow \tilde{b}_1 W)$ , it can be obtained in analogous to Eq. (21) after the replacements  $\cos \theta_{\tilde{t}} \rightarrow \sin \theta_{\tilde{t}}$  and  $\tilde{b}_1 \rightarrow \tilde{t}_2$ ,  $\tilde{t}_1 \rightarrow \tilde{b}_1$ . And its branching ratio is smaller than 40%.

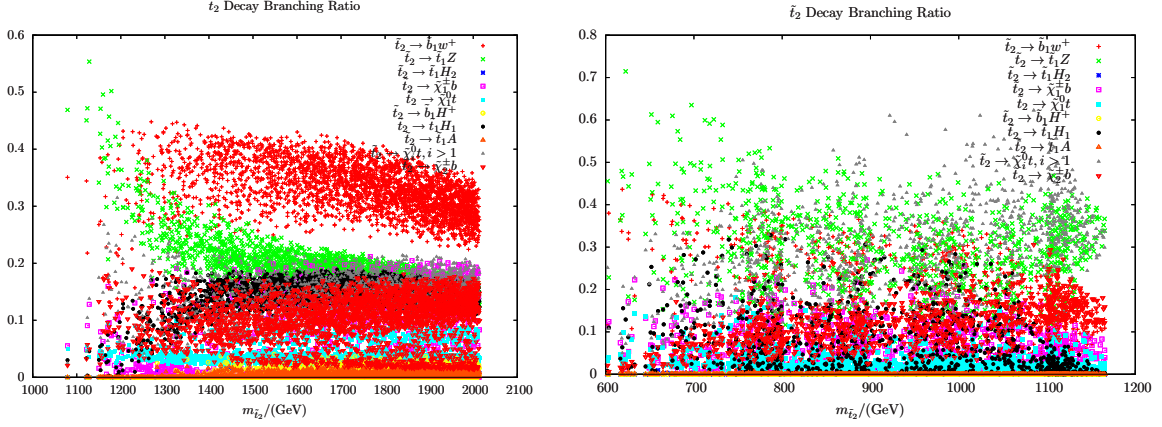


FIG. 6: Plots of decay branching ratios of  $\tilde{t}_2$ . Left: MSSM; Right: NMSSM.

## B. Explore the heavier stop and sbottom LHC signatures

With the aid of the results in the previous subsection, we now attempt to preliminarily explore the characteristic signatures for the stop ensemble at the LHC. We will not devote ourself to  $\tilde{t}_1$ , which has been the focus of many works. The decays of heavier states  $\tilde{t}_2$  and  $\tilde{b}_1$  may give rise to novel collider signatures, which potentially provide a way to probe the stop ensemble rather than  $\tilde{t}_1$  alone. Signatures of stops/sbottom strongly depend on the decay chains of neutralinos/charginos, which however are not specified in this work. They can be very different in different SUSY scenarios. For example, in certain  $R$ -parity-violating SUSY, the large missing energy is absent and consequently most of the current stop searches are invalid. In what follows we present several categories of signatures.

**Same-sign dilepton (SSDL) & Multi-leptons (MLs)** Signatures containing SSDL or MLs are common to several channels, thanks to the hard  $W$  or/and  $Z$  bosons generated during the cascade decays of the heavier stop/sbottom to the lighter states. SSDL is rare in the SM, so it provides a promising avenue for observing the additional third family colored sparticles.

Considering the relatively heavy  $\tilde{b}_1$  pair production and at least one  $\tilde{b}_1$  decays along the chain (We use superscript “ $\pm$ ” to denote the sign of charge, discarding its value):

$$\tilde{b}_1^- \rightarrow \tilde{t}_1 (\rightarrow \sum_{i \geq 1} \tilde{\chi}_i^0 + W^+ + b^-) + W^-, \quad (25)$$

which produces a pair of opposite-sign dibosons. According to the previous numerical results, the other sbottom  $\tilde{b}_1^+$  dominantly decays into either  $\tilde{t}_1^- W^+$  or  $\tilde{\chi}^+ t^-$ . Combining with the products of  $\tilde{b}_1^-$  decay, in any case one gets the same-sign dibosons with an appreciable cross section. Actually, we can even get  $W^+ W^+$  plus  $W^- W^-$ , but with a

significantly reduced cross section.  $\tilde{t}_2$  decay is also a rich source of SSDL. Similarly, considering the pair production of  $\tilde{t}_2$ , followed by at least one of them decays as:

$$\begin{aligned}\tilde{t}_2^+ &\rightarrow \tilde{t}_1(\rightarrow \tilde{\chi}^0 + W^+ + b^-) + Z, \\ &\rightarrow \tilde{b}_1 [\tilde{t}_1(\rightarrow \tilde{\chi}^0 + W^+ + b^-) + W^-] + W^+.\end{aligned}\quad (26)$$

Each chain itself produces SSDL, and thus if we inclusively observe the SSDL, the LHC sensitivity can be substantially improved.

We would like to give several comments. In the first, the  $W/Z$ -richness in the above decay chains means that final states may be lepton rich, so multi-leptons (MLS) deserve attentions. Next, we do not take the neutralinos and charginos decays into account. Actually, charged leptons are likely to be produced, mediated by the on- or off-shell  $W(Z)$ -bosons, in the  $\chi^\pm(\chi_i^0)$  cascade decays. So  $\tilde{t}_2 \rightarrow \sum_{i \geq 2} \chi_i^0 t$  and  $\tilde{b}_1 \rightarrow \chi_1^\pm t$ , which have large branching ratios, provide SSDL also. Finally, the current CMS searches for the SSDL accompanied by at least two  $b$ -jets [31], and signatures are divided into categories both with and without large MET. SSDL from  $\tilde{t}_2/\tilde{b}_1$  decay satisfies the criterion and is thus subject to the CMS constraint. In some case, the  $\sqrt{s} = 8$  TeV and the  $\mathcal{L} = 10.5 \text{ fb}^{-1}$  data has already set a lower bound of 450 GeV on  $\tilde{b}_1$  [31].

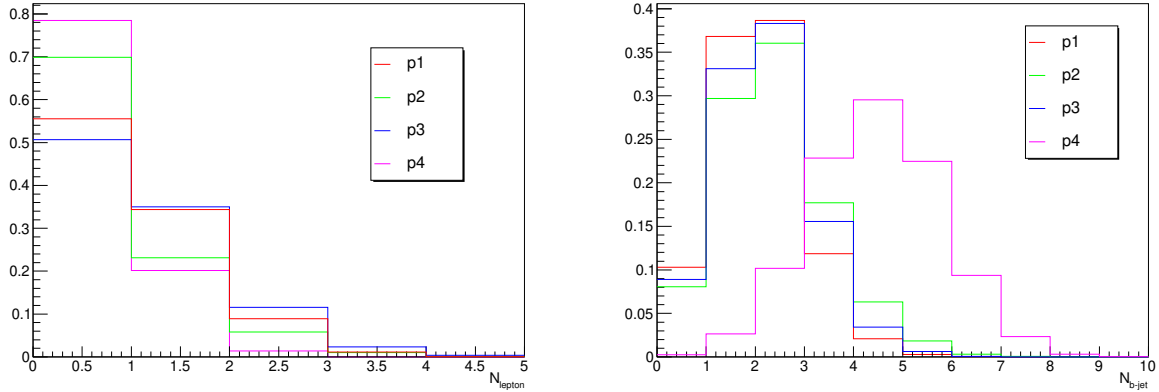


FIG. 7: Distribution of the numbers of leptons  $N_{lepton}$  and  $b$ -jets  $N_{b-jet}$  for the four benchmark points. The vertical axis denotes the number of events, in unit 50000 (same in Fig. 8).

**Multi  $b$ -jets** Top quark and  $Z/h$  are sources of  $b$ -jet. So, it is expected that multi  $b$ -jets (no less than 3) signature is produced in the stop ensemble. This signature alone is powerful. For example, it helps to discover  $t'$  with mass  $\lesssim 550$  GeV at  $5\sigma$  level [32]. Here, it can be further strengthened by assistant cuts such as a large MET and thus vigorously probes the heavier stop/sbottom. As before, we do not need to specify the neutralino/chargino decays.

This signature is especially suited for searching  $\tilde{t}_2$ . Still considering the  $\tilde{t}_2$  pair production, the pattern of subsequent decay is

$$\tilde{t}_2 \rightarrow \tilde{t}_1 + Z/h \rightarrow 3b + X \quad \text{and} \quad \tilde{t}_2 \rightarrow b + X, \quad (27)$$

Since  $\tilde{t}_2$  decay produces at least one hard  $b$ -jet, so  $\text{Br}(\tilde{t}_2 \rightarrow b + X)$  does not suffer suppression from branching ratios. Similar search strategy has been adopted in Ref. [33, 34], where the jet substructure of  $b\bar{b}$  from  $h$  or  $Z$  decay is used to enhance the signal sensitivity. Pair production of  $\tilde{b}_1$  can not give rise to the multi hard  $b$ -jets signature except for taking into account the  $Z/h$  bosons from the heavier neutralino decays.

We note that the signature  $2b$ -jets+MET has been utilized by CMS and ATLAS [35] to search sbottom with decay mode  $\tilde{b}_1 \rightarrow \chi_1^0 b$ . Although it is a strong signature of  $\tilde{t}_2/\tilde{b}_1$ , the present searches hardly constrain the stop ensemble in this paper. The reason is that, on the one hand, the mode  $\tilde{b}_1 \rightarrow \chi_1^0 b$  is subdominant for heavier  $\tilde{b}_1$ ; On the other hand, to suppress the huge  $t\bar{t}$  background, they veto leptons which however are generic from the  $\tilde{t}_2/\tilde{b}_1$  decays.

**Boosted tops** Top quarks appear in the most decay chains of  $\tilde{t}_2/\tilde{b}_1$ . Thereby, for the stop ensemble lies in the heavier region, says close to the TeV scale, signatures containing boosted tops are well expected. Boosted tops can be produced from the primary of  $\tilde{t}_2/\tilde{b}_1$ , via  $\tilde{t}_2 \rightarrow t\tilde{\chi}_i^0$  and  $\tilde{b}_1 \rightarrow \tilde{\chi}_i^\pm b$ , or from their secondary decay as shown in the benchmark points. But the latter case only produces moderately boosted tops with  $p_T \sim 200$  GeV, given  $\tilde{t}_1$  around 500 GeV. They can be tagged using heptotagger [37]. For  $p_T \gtrsim 200$  GeV, the top tagger efficiency is around 30% or even higher [37]. However, top-tagging alone fails to kill the huge backgrounds from  $t\bar{t}$  production. So we may need the help from other variables, e.g.,  $m_{T2}$ . Because of the heaviness of mother particles, the signatures have much larger  $m_{T2}$  than that of the  $t\bar{t}$  background [36].

To form an initial impression on the LHC prospects of the characterized signatures originating from decays between stop and sbottom, we consider four benchmark points, which are listed in the second and third columns of Table. I. Each step along the decay chain has been assumed to have a 100% branching ratio, except for the well known particles  $t$ ,  $W$  and  $Z$ , which decay in PYTHIA. For each point, 50000 events at the 14 TeV LHC are generated by MadGraph5 [38], and passed to PYTHIA6 [39] for particle decay and parton shower. The detector effects are implemented by Delphes3 [40].

We start from SSDL. We adopt the ATLAS definition of SSDL [41], which requires two leading isolated leptons with  $p_T > 20$  GeV and  $|\eta| < 2.47$  for electron while  $|\eta| < 2.4$  for

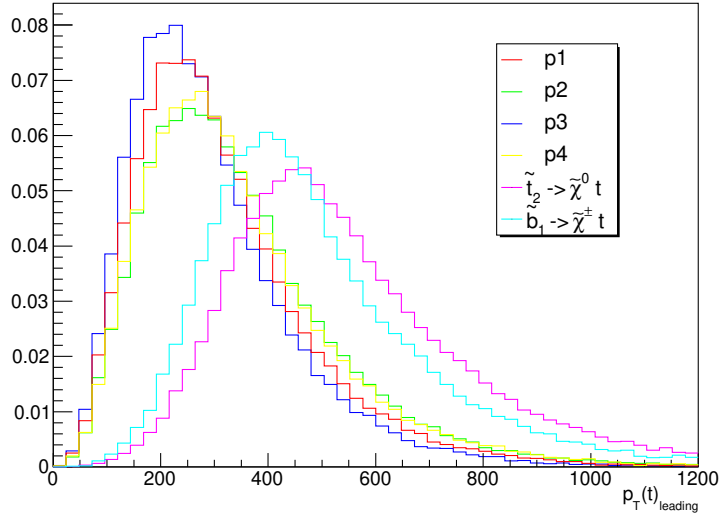


FIG. 8: Distribution of  $p_T$  of top quark in each benchmark points and from the ordinary decay channels, i.e., these with primary top quark. Here both  $\tilde{\chi}^0$  and  $\tilde{\chi}^\pm$  have mass 100 GeV.

	Channel	Masses	$R_{\text{SSDL}}$	$N_{\text{SSDL}}/100fb^{-1}$
$p_1$	$\tilde{b}_1 \rightarrow \tilde{t}_1 W^- \rightarrow (t\tilde{\chi}_1^0)W^-$	$m_{\tilde{b}_1} = 800 \text{ GeV}$	$\frac{1680}{50000}$	116.9
$p_2$	$\tilde{t}_2 \rightarrow \tilde{t}_1 Z \rightarrow (t\tilde{\chi}_1^0)Z$	$m_{\tilde{t}_2} = 900 \text{ GeV}$	$\frac{477}{50000}$	15.0
$p_3$	$\tilde{t}_2 \rightarrow \tilde{b}_1 W^+ \rightarrow (\tilde{t}_1 W^-)W^+ \rightarrow (t\tilde{\chi}_1^0 W^-)W^+$	$m_{\tilde{t}_2} = 900 \text{ GeV}, m_{\tilde{b}_1} = 700 \text{ GeV}$	$\frac{2817}{50000}$	88.5
$p_4$	$\tilde{t}_2 \rightarrow \tilde{t}_1 h \rightarrow (t\tilde{\chi}_1^0)(b\bar{b})$	$m_{\tilde{t}_2} = 900 \text{ GeV}$	$\frac{4}{50000}$	0.1

TABLE I:  $m_{\tilde{\chi}_1^0} = 100 \text{ GeV}$ ,  $m_{\tilde{t}_1} = 400 \text{ GeV}$

muon which carries the same electric charge with the electron. Lepton isolation requires that, inside a cone of  $R = 0.15$  around this lepton, the scalar sum of  $p_T$  of the final particles is less than 10% of  $p_{T,\text{lepton}}$ . The rates of SSDL in each benchmark point are given in Table I, the fourth column. We can understand the results via the naive estimation like

$$R_{\text{SSDL}}(p_1) \simeq 2\text{Br}(W_\ell)^2 \mathcal{P}_1, \quad (28)$$

with the  $W_\ell$  and  $Z_\ell$  leptonic decay branching ratios about 1/5 and 1/10, respectively. Then it is seen that the probability of SSDL  $\mathcal{P}_1 \sim 50\%$ , a remarkably high probability. Given SSDL rates, we estimate the corresponding numbers of events at the 14 TeV LHC with integrated luminosity  $100 \text{ fb}^{-1}$  (We calculate the production cross sections using [42]). The results are listed in the last column of Table I. As one can see,  $p_1$  and  $p_3$ , namely both  $\tilde{b}_1$  and  $\tilde{t}_2$ , have a good chance to be discovered. As for the MLs, its rate is suppressed by the decay branching ratios and thus is not that attractive, see the right panel of Fig. 7. We now turn our attention to the multi  $b$ -jets. We include a  $b$ -tagging efficiency of 70% and a probability

of 10% and 1% for mis-tagging a charm quark and other light quarks, respectively. The distributions of  $b$ -jets numbers  $N_b$  are displayed in the left panel of Fig. 7. From it one can see that, all the benchmark points are  $b$ -rich ( $N_b \geq 2$ ), and especially, the number of  $b$ -jets of  $p_4$  peaks at 4. Finally, we plot the  $p_T$  distribution of top quark, in Fig. 8. It shows that, as expected, top from secondary decay is moderately boosted, with (leading top)  $p_T$  slightly above  $m_{\tilde{t}_1}/2$ , while the primary top quark is highly boosted with  $p_T$  peaks at half of the mother particle mass. In summary, the stop ensemble closing 1 TeV can be probed via SSDL, multi  $b$ -jets or boosted top. But here we only make the preliminary analysis of the signature properties, and the quantitative collider study, like improved cuts and backgrounds analysis, is left for future work.

#### IV. CONCLUSIONS AND DISCUSSIONS

As the LHC data accumulates, it is likely to show us a sterile Higgs boson. That is to say, its (main) signature strengths deviating from the SM predictions are within the experimental resolution ( $\lesssim 10\%$ ). Recalling that in the SSM Higgs couplings are often modified by mixing and stops, Higgs sterility should have a deep implication on the Higgs and stop sector. We analyzed that based on two benchmark models:

- In the nearly decoupling region of MSSM, the doublet-doublet mixing effect is universal up to an individual enhancement in  $C_{hb\bar{b}}$ , by  $2m_Z^2/M_A^2$ . Higgs sterility then places a bound:  $M_A \gtrsim 900$  GeV. Since  $m_h \simeq 126$  GeV relies on a heavy stop sector, then to get a relatively light stop we should turn to large stop mixing or/and asymmetric stop soft mass squared. Such cases are subject to constraint from the Higgs sterility. But generically sterility does not mean much to the stop sector.
- Similarly, in the NMSSM violation of universality of the Higgs mixing effect is encoded in  $C_{hb\bar{b}}$ . However, here  $C_{hb\bar{b}}$  can be made either smaller or larger than 1, due to the distortion of doublet-doublet mixing effect by DSM. Interestingly, given a large  $\tan\beta$  the DSM effect may not simply vanish as  $M_A$  increases. Moreover, depending on the structure of the Higgs sector, the DSM effect can push-up  $m_h$  or pull-down  $m_h$ . In the former scenario, the amount of pushing-up is less than  $\sim 5$  GeV due to sterility. In particular, we revise to the pushing-up region with a large  $\tan\beta$  and moderately small  $\lambda$ , which may help to embed the low energy NMSSM into the (semi)constrained form [43]. In the pulling-down scenario, Higgs sterility is automatically implemented, because to weaken the pulling-down effect DSM is strongly favored to be small. In any case, stops in the NMSSM are allowed to be comparatively light, so Higgs sterility both directly and indirectly constrains them.



We have to emphasize that we here focus on the tree-level analysis. The full supersymmetric QCD correction (In this paper it is only partially included because we fixed many relevant parameters, like the gluino mass.) may change  $C_{h\bar{b}b}$  substantially [44, 45]. However, radiative correction strongly depends on the total soft spectrum, which renders a generic prediction very difficult.

We also studied the LHC features of the whole stop sector, rather than merely the lightest stop (A work in this inspirit has appeared [46].), allowed by a 126 GeV sterile Higgs boson. We first made a detailed numerical analysis of the stop sector of the NMSSM, including the mass and decay distributions of  $\tilde{t}_2$  and  $\tilde{b}_1$ . Then we propose several promising signatures for discovering the heavier stop and sbottom. Due to the cascade decays among stops and sbottom, same sign leptons and multi- $b$  jets are characterized signatures and have promising prospect at the future LHC.

To end up this work, we add several remarks. First, although a lot of papers have studied the mixing effect(s) in the (N)MSSM, our paper reveals their most remarkable features and clarifies some points which seem to be unclear in the literatures. Additionally, the idea of using Higgs sterility to constrain new physics, of course, can be generalized to many other contexts where Higgs couplings are modified [47–49]. As the final remark, we would like to stress that our discussions on characteristic signatures of the heavier stop/light sbottom actually are based on SUSY with less fine-tuning, so our work may open a new window to probe natural SUSY. But the results presented in this paper are preliminary, and their actual prospects need more detailed LHC analysis, and we leave it for an open question.

## V. ACKNOWLEDGEMENTS

We would like to thank Taoli Cheng for helpful discussions. This research was supported in part by the China Postdoctoral Science Foundation under grant numbers 2013M530006 (KZ), and by the Natural Science Foundation of China under grant numbers 10821504, 11075194, 11135003, and 11275246.

### Appendix A: Higgs effective couplings

In this appendix we briefly introduce how to construct effective couplings of the SM-like Higgs boson  $h_{\text{SM}}$ . We start from the Lagrangian with tree-level couplings only:

$$\mathcal{L}_{\text{tree}} \supset r_{i,Z} \frac{M_Z^2}{\sqrt{2}v} H_i Z Z + r_{i,W} \frac{\sqrt{2}M_W^2}{v} H_i W^+ W^- - r_{i,f} \frac{m_f}{\sqrt{2}v} H_i \bar{f} f - r_{i,S} \frac{\sqrt{2}m_S^2}{v} H_i S^\dagger S, \quad (\text{A1})$$

with  $v \approx 174$  GeV. In the NMSSM, we have  $h_{\text{SM}} = H_i$  with  $i = 1$  or  $2$ . Here  $f$  and  $S$  denote a Dirac fermion and complex scalar, respectively. For the particles belonging to the SM, the

dimensionless parameters  $r_{i,V}$ , etc., can measure the deviations of  $H_i$  from  $h_{\text{SM}}$ . They are supposed to slide to 1 when  $H_i$  exactly coincides with  $h_{\text{SM}}$ .

In Eq. (A1), particles carrying QCD or/and QED charges generate Higgs effective couplings to gluons and photons at loop level. They are crucial to the detection of Higgs boson at the LHC, and incorporated through the following dimension-five operators [50]:

$$\mathcal{L}_{\text{loop}} = r_{i,g} \frac{\alpha_s}{12\sqrt{2}v} H_i G_{\mu\nu}^a G^{a,\mu\nu} + r_{i,\gamma} \frac{\alpha}{\sqrt{2}v} H_i F_{\mu\nu} F^{\mu\nu}. \quad (\text{A2})$$

Note that in this notation  $r_{i,g}$  and  $r_{i,\gamma}$  are not 1 in the SM limit. The operator coefficients can be calculated in terms of the following formulas (See Ref. [9] and references therein):

$$\begin{aligned} r_g &= \frac{C_2(r_s)}{2} r_s \mathcal{A}_s(\tau_s) + 2C_2(r_f) r_f \mathcal{A}_f(\tau_f), \\ r_\gamma &= \frac{N(r_s)Q_s^2}{24} r_s \mathcal{A}_s(\tau_s) + \frac{N(r_f)Q_f^2}{6} r_f \mathcal{A}_f(\tau_f) - \frac{7Q_V^2}{8} r_V \mathcal{A}_V(\tau_V), \end{aligned} \quad (\text{A3})$$

where  $C_2(r)$  and  $N(r)$  are the quadratic Casimir and number of colors of the representation  $r$  under  $SU(3)_C$ . For a heavy particle with  $\tau \equiv m_h^2/4m^2 \ll 1$ , its loop function  $\mathcal{A} \rightarrow 1$  and the corresponding contribution is then fixed up to the parameter  $r$ . Within the SM, the top quark and  $W$ -boson dominantly account for Eq. (A2). In the (N)MSSM we have

$$\begin{aligned} r_{i,g} &\approx 1.03 r_{i,t} - 0.06 r_{i,b} + \delta r_{i,g}(\text{stops}), \\ r_{i,\gamma} &\approx \frac{2}{9} \times 1.03 r_{i,t} - 1.04 r_{i,V} + \delta r_{i,\gamma}(\text{stops, chargino}). \end{aligned} \quad (\text{A4})$$

To get them we have taken  $m_{H_i} \simeq 126$  GeV. For the exact SM Higgs boson, i.e.,  $H_i = h_{\text{SM}}$  we have  $r_{\text{SM},g} = 0.97$  and  $r_{\text{SM},\gamma} = -0.81$ .

To compare with experimental data, it is convenient to express Higgs signature strengths in terms of  $r$ . For example, for  $X = (2\gamma, VV, b\bar{b}, \dots)$  from the gluon fusion channel we have

$$R_{gg}^{H_i}(X) \equiv \frac{\Gamma(H_i \rightarrow gg) \text{Br}(H_i \rightarrow X)}{\Gamma(h_{\text{SM}} \rightarrow gg) \text{Br}(h_{\text{SM}} \rightarrow X)} = \frac{r_{i,g}^2}{r_{\text{SM},g}^2} \frac{r_{i,X}^2}{r_{\text{SM},X}^2} \frac{1}{B_{\text{tot}}}, \quad (\text{A5})$$

with  $C_{\text{tot}}$  the ratio of total decay widths, i.e.,  $\Gamma_{H_i}/\Gamma_{h_{\text{SM}}}$ . Signature strengths from other channels can be defined similarly. In literatures such as the NMSSMTools [24], the reduced couplings  $C_{i,X} \equiv r_{i,X}/r_{\text{SM},X}$  are used. With this notation,  $R_{gg}^{H_i}(X) = C_{i,g}^2 C_{i,X}^2 / B_{\text{tot}}$  with

$$B_{\text{tot}} \approx 0.64 C_{i,b}^2 + 0.24 C_{i,V}^2 + 0.09 C_{i,g}^2 + 0.03 C_{i,t}^2 \leq 1. \quad (\text{A6})$$

To derive it we have used:  $\text{Br}(h_{\text{SM}} \rightarrow b\bar{b} + \tau\bar{\tau}) = 0.64$ ,  $\text{Br}(h_{\text{SM}} \rightarrow WW^* + ZZ^*) = 0.24$ ,  $\text{Br}(h_{\text{SM}} \rightarrow gg) = 0.085$  and  $\text{Br}(h_{\text{SM}} \rightarrow c\bar{c}) = 0.027$ .

## Appendix B: The Higgs and stop mass square matrices

In the basis  $(S_1, S_2, S_3)$  defined in the text, the elements of the CP-even Higgs mass square matrix  $M_S^2$  are given by

$$\begin{aligned}
(M_S^2)_{11} &= M_A^2 + (m_Z^2 - \lambda^2 v^2) \sin^2 2\beta, & (M_S^2)_{12} &= -\frac{1}{2}(m_Z^2 - \lambda^2 v^2) \sin 4\beta, \\
(M_S^2)_{13} &= -\frac{1}{2}(M_A^2 \sin 2\beta + 2\lambda\kappa v_s^2) \cos 2\beta \frac{v}{v_s}, & (M_S^2)_{22} &= m_Z^2 \cos^2 2\beta + \lambda^2 v^2 \sin^2 2\beta, \\
(M_S^2)_{23} &= \frac{1}{2}(4\lambda^2 v_s^2 - M_A^2 \sin^2 2\beta - 2\lambda\kappa v_s^2 \sin 2\beta) \frac{v}{v_s}, \\
(M_S^2)_{33} &= \frac{1}{4}M_A^2 \sin^2 2\beta \left(\frac{v}{v_s}\right)^2 + 4\kappa^2 v_s^2 + \kappa A_\kappa v_s - \frac{1}{2}\lambda\kappa v^2 \sin 2\beta,
\end{aligned} \tag{B1}$$

where  $M_A^2 = 2\lambda v_s(A_\lambda + \kappa v_s)/\sin 2\beta$ . Using it, we can rewrite  $(M_S^2)_{23,33}$  as

$$\begin{aligned}
(M_S^2)_{23} &= 2\lambda\mu\nu \left[ 1 - \left( \frac{A_\lambda}{2\mu} + \frac{\kappa}{\lambda} \right) \sin 2\beta \right], \\
(M_S^2)_{33} &= \lambda^2 v^2 \frac{A_\lambda}{2\mu} \sin 2\beta + 4\frac{\kappa^2}{\lambda^2} \mu^2 + \frac{\kappa}{\lambda} A_\kappa \mu.
\end{aligned} \tag{B2}$$

The stop sector has three parameters, casted in the stop mass square matrix  $M_{S_{stop}}^2$ . In the basis  $(\tilde{t}_R, \tilde{t}_L)$ , it takes the form of

$$M_{S_{stop}}^2 = \begin{pmatrix} m_{\tilde{t}_R}^2 + m_t^2 - (v_u^2 - v_d^2)g_1^2/3 & m_t(A_t - \mu \cot \beta) \\ m_{\tilde{t}_L}^2 + m_t^2 + (v_u^2 - v_d^2)(g_1^2/12 + g_2^2/4) \end{pmatrix}. \tag{B3}$$

We define the first and second diagonal entries of  $\mathcal{M}_{stop}^2$  as  $m_{RR}^2$  and  $m_{LL}^2$ , respectively. The mass eigenstates are denoted as  $\tilde{t}_{1,2}$ , and the corresponding eigenvalues are

$$m_{\tilde{t}_{1,2}}^2 = \frac{1}{2} \left[ (m_{LL}^2 + m_{RR}^2) \mp \sqrt{(m_{LL}^2 - m_{RR}^2)^2 + 4X_t^2 m_t^2} \right], \tag{B4}$$

with  $X_t \equiv A_t - \mu \tan \beta$ . The flavor and mass eigenstates are related by

$$\tilde{t}_L = \cos \theta_{\tilde{t}} \tilde{t}_1 - \sin \theta_{\tilde{t}} \tilde{t}_2, \quad \tilde{t}_R = \sin \theta_{\tilde{t}} \tilde{t}_1 + \cos \theta_{\tilde{t}} \tilde{t}_2, \tag{B5}$$

with the stop mixing angle  $\theta_{\tilde{t}}$  defined through  $\tan 2\theta_{\tilde{t}} = 2X_t m_t / (m_{LL}^2 - m_{RR}^2)$ . Thereby, the degeneracy between  $m_{RR}^2$  and  $m_{LL}^2$ , or/and large left-right stop mixing  $X_t$  lead to  $\theta_{\tilde{t}} \rightarrow \pi/4$ .

- [1] G. Aad et al. [ATLAS Collaboration], Phys. Lett. B 716, 1 (2012); S. Chatrchyan et al. [CMS Collaboration], Phys. Lett. B 716, 30 (2012).
- [2] N. Mohr [on behalf of the CMS Collaboration], arXiv:1307.5745 [hep-ex].

- [3] M. E. Peskin, arXiv:1207.2516.
- [4] U. Ellwanger, C. Hugonie and A. M. Teixeira, Phys. Rept. **496**, 1 (2010).
- [5] Z. Kang, Y. Liu and G. -Z. Ning, arXiv:1301.2204.
- [6] J. R. Espinosa and M. Quiros, Phys. Lett. B **279**, 92 (1992); T. Basak and S. Mohanty, Phys. Rev. D **86**, 075031 (2012); A. Delgado, G. Nardini and M. Quiros, arXiv:1207.6596.
- [7] A. Djouadi, Phys. Rept. **459**, 1 (2008).
- [8] A. Arbey, M. Battaglia and F. Mahmoudi, Phys. Rev. D **88**, 015007 (2013).
- [9] D. Carmi, A. Falkowski, E. Kuflik, T. Volansky and J. Zupan, JHEP **1210**, 196 (2012).
- [10] M. A. Ajaib, I. Gogoladze and Q. Shafi, Phys. Rev. D **86**, 095028 (2012).
- [11] Z. Kang, J. Li and T. Li, JHEP **1211**, 024 (2012).
- [12] L. J. Hall, D. Pinner and J. T. Ruderman, JHEP **1204**, 131 (2012), 1112.2703; B. Kyae and J. -C. Park, Phys. Rev. D **87**, 075021 (2013); T. Gherghetta, B. von Harling, A. D. Medina and M. A. Schmidt, JHEP **1302**, 032 (2013).
- [13] D. J. Miller, R. Nevzorov and P. M. Zerwas, Nucl. Phys. B **681**, 3 (2004).
- [14] Z. Kang, J. Li, T. Li, D. Liu and J. Shu, arXiv:1301.0453.
- [15] N. D. Christensen, T. Han, Z. Liu and S. Su, arXiv:1303.2113.
- [16] K. Choi, S. H. Im, K. S. Jeong and M. Yamaguchi, arXiv:1211.0875; C. Cheung, S. D. McDermott and K. M. Zurek, JHEP **1304**, 074 (2013);
- [17] S. Chang, P.J. Fox and N. Weiner, JHEP **08** (2006) 068; R. Dermisek and J.F. Gunion, Phys. Rev. D **77** (2008) 015013.
- [18] J. -J. Cao, Z. -X. Heng, J. M. Yang, Y. -M. Zhang and J. -Y. Zhu, JHEP **1203**, 086 (2012); K. S. Jeong, Y. Shoji and M. Yamaguchi, JHEP **1209**, 007 (2012); K. Agashe, Y. Cui and R. Franceschini, arXiv:1209.2115; T. Cheng and T. Li, arXiv:1305.3214; S. F. King, M. Mhlleitner, R. Nevzorov and K. Walz, Nucl. Phys. B **870**, 323 (2013);
- [19] D. G. Cerdeno, P. Ghosh and C. B. Park, JHEP **1306**, 031 (2013); R. Barbieri, D. Buttazzo, K. Kannike, F. Sala and A. Tesi, arXiv:1307.4937; U. Ellwanger, arXiv:1306.5541; D. G. Cerdeno, P. Ghosh, C. B. Park and M. Peiro, arXiv:1307.7601; J. Hasenkamp and M. W. Winkler, arXiv:1308.2678.
- [20] U. Ellwanger, arXiv:1112.3548; R. Benbrik, M. Gomez Bock, S. Heinemeyer, O. Stal, G. Weiglein and L. Zeune, Eur. Phys. J. C **72**, 2171 (2012); C. Beskidt, W. de Boer and D. I. Kazakov, arXiv:1308.1333.
- [21] S. Schael *et al.* [ALEPH and DELPHI and L3 and OPAL and LEP Working Group for Higgs Boson Searches Collaborations], Eur. Phys. J. C **47**, 547 (2006).
- [22] A. Djouadi, J. Kalinowski and M. Spira, Comput. Phys. Commun. **108**, 56 (1998) .
- [23] A. Belyaev, N. D. Christensen and A. Pukhov, Comput. Phys. Commun. **184**, 1729 (2013).

- [24] U. Ellwanger and C. Hugonie, *Comput. Phys. Commun.* **175** (2006) 290; U. Ellwanger, J. F. Gunion, and C. Hugonie, *JHEP* **02** (2005) 066.
- [25] L. Aparicio, P. G. Camara, D. G. Cerdeno, L. E. Ibanez and I. Valenzuela, *JHEP* **1302**, 084 (2013).
- [26] ATLAS Collaboration, ATLAS-CONF-2013-053.
- [27] ATLAS Collaboration, ATLAS-CONF-2013-037; ATLAS Collaboration, ATLAS-CONF-2013-048; CMS Collaboration, CMS-PAS-SUS-13-011.
- [28] X. -J. Bi, Q. -S. Yan and P. -F. Yin, arXiv:1209.2703; J. Cao, C. Han, L. Wu, J. M. Yang and Y. Zhang, *JHEP* **1211**, 039 (2012); T. Cheng, J. Li, T. Li and Q. -S. Yan, arXiv:1304.318.
- [29] M. Badziak, M. Olechowski and S. Pokorski, arXiv:1304.5437.
- [30] A. Arhrib and R. Benbrik, *Phys. Rev. D* **71**, 095001 (2005).
- [31] S. Chatrchyan *et al.* [CMS Collaboration], *JHEP* **1303**, 037 (2013).
- [32] K. Harigaya, S. Matsumoto, M. M. Nojiri and K. Tobioka, *Phys. Rev. D* **86**, 015005 (2012).
- [33] D. Berenstein, T. Liu, E. Perkins and , arXiv:1211.4288 [hep-ph].
- [34] D. Ghosh, arXiv:1308.0320 [hep-ph].
- [35] ATLAS Collaboration, ATLAS-CONF-2012-165; S. Chatrchyan *et al.* [CMS Collaboration], arXiv:1303.2985.
- [36] A. Chakraborty, D. K. Ghosh, D. Ghosh and D. Sengupta, arXiv:1303.5776.
- [37] T. Plehn, M. Spannowsky, M. Takeuchi and D. Zerwas, *JHEP* **1010**, 078 (2010).
- [38] J. Alwall, M. Herquet, F. Maltoni, O. Mattelaer and T. Stelzer, *JHEP* **1106**, 128 (2011).
- [39] T. Sjostrand, S. Mrenna and P. Z. Skands, *JHEP* **0605**, 026 (2006).
- [40] J. de Favereau, C. Delaere, P. Demin, A. Giammanco, V. Lematre, A. Mertens and M. Selvaggi, arXiv:1307.6346 [hep-ex].
- [41] ATLAS Collaboration, ATLAS-CONF-2013-007.
- [42] W. Beenakker, R. Hopker and M. Spira, hep-ph/9611232.
- [43] J. F. Gunion, Y. Jiang and S. Kraml, *Phys. Lett. B* **710**, 454 (2012); U. Ellwanger and C. Hugonie, *Adv. High Energy Phys.* **2012**, 625389 (2012); K. Kowalska, S. Munir, L. Roszkowski, E. M. Sessolo, S. Trojanowski and Y. -L. S. Tsai, arXiv:1211.1693; D. Das, U. Ellwanger and A. M. Teixeira, *JHEP* **1304**, 117 (2013).
- [44] C. Han, X. Ji, L. Wu, P. Wu and J. M. Yang, arXiv:1307.3790.
- [45] M. Cahill-Rowley, J. Hewett, A. Ismail and T. Rizzo, arXiv:1308.0297.
- [46] G. D. Kribs, A. Martin and A. Menon, arXiv:1305.1313.
- [47] B. Batell, D. McKeen and M. Pospelov, *JHEP* **1210**, 104 (2012); D. Bertolini and M. McCullough, *JHEP* **1212**, 118 (2012).
- [48] S. Chpoi, S. Jung and P. Ko, arXiv:1307.3948.

- [49] D. Lopez-Val, T. Plehn and M. Rauch, arXiv:1308.1979.
- [50] M. A. Shifman, A. I. Vainshtein, M. B. Voloshin and V. I. Zakharov, Sov. J. Nucl. Phys. 30, 711 (1979) [Yad. Fiz. 30, 1368 (1979)].
- [51] Such a prediction is of great importance to find a smoking gun for the exotic Higgs bosons in the MSSM. As far as our knowledge, this point is not explicitly pointed out by any reference, despite of a relevant study [8]. We leave a specific study about it elsewhere.
- [52] How to detect this light Higgs boson, or more broadly speaking the extra light Higgs states predicted in the NMSSM, is challenging but interesting [14, 15, 19].
- [53] Such a scenario was briefly discussed in Ref. [11] and then numerically studied by Ref. [25, 29]. Here we present a more detailed numerical analysis.